RSC Advances

PAPER

View Article Online
View Journal | View Issue

Cite this: *RSC Adv.*, 2019, **9**, 15868

Heteroatom-doped hollow carbon spheres made from polyaniline as an electrode material for supercapacitors

Haiyan Liu,[a] Mei Han,[a] Jinzong Zuo,[a] Xuexiang Deng,[a] Wenxue Lu,[a] Yongguo Wu,[a] Huaihe Song, *[b] Chunli Zhou[b] and Shengfu Ji[b]

Received 10th April 2019
Accepted 13th May 2019

DOI: 10.1039/c9ra02685a

rsc.li/rsc-advances

In this work, novel heteroatom-doped hollow carbon spheres (HHCSs) were prepared *via* the carbonization of polyaniline hollow spheres (PHSs), which were synthesized by one-pot polymerization. It was found that the carbonized PHSs at 700 °C exhibit high specific capacitance of 241 F g^{-1} at a current density of 0.5 A g^{-1} and excellent rate capability. The excellent electrochemical performance can be attributed to the heteroatom-doping and hollow carbon nanostructure of the HHCSs electrodes. Heteroatom groups in the HHCSs not only improve the wettability of the carbon surface, but also enhance the capacitance by addition of a pseudocapacitive redox process. Their unique structure provides a large specific surface area along with reduced diffusion lengths for both mass and charge transport.

1. Introduction

Supercapacitors are great potential energy storage devices with unique dual advantages of both traditional dielectric capacitors and rechargeable batteries. They can transport high power within a very short period, store high energy, and exhibit long cycle life.[1–3] According to the mechanism of charge storage, supercapacitors can be divided into two types: electric double-layer capacitors (EDLCs) and pseudocapacitors. The former can store energy through the separation of electronic and ionic charges at the interface between an electrode and an electrolyte solution and the latter has faradaic reactions on the electrode materials.

Various types of carbon materials meeting the mechanism of the EDLCs have been used as electrode materials, such as activated carbons,[4,5] carbon nanotubes,[6] graphene,[7] carbon aerogels[8] and mesoporous carbons.[9] Carbon-based electrode materials can offer lower specific capacitance and energy density in supercapacitor compared with most pseudocapacitor electrode materials such as metal oxides and conductive polymers. Doping carbonaceous materials with heteroatoms can couple the pseudocapacitance to the EDLCs while maintaining the excellent intrinsic characteristics of carbonaceous materials at the same time. Recently, many attempts have been devoted to the preparation of heteroatom-doped carbon-based materials.[10–15] For example, heteroatom-doped carbonaceous materials have been obtained from gelatin,[16] leaves,[17] animal bones,[18] banana fibers,[19] rice husk,[20] catkins[21] and so on.

In addition to heteroatoms doping, an appropriate microstructure can improve the electrochemical performance of carbonaceous materials by providing high electrochemically accessible surface area.[22] Hollow spheres are promising microstructure due to their high surface-to-volume ratios and reduced transport lengths for both mass and charge transport.[23–27] Dong *et al.* reported a surfactant-assisted template method for synthesis of hollow carbon nanospheres by using polydopamine (PDA) as carbon source and ZnO as template.[26] Nitrogen-containing carbon microspheres with hollow core exhibit the specific capacitance of 306 F g^{-1} at a current density of 0.1 A g^{-1} in 2 M H_2SO_4.[27] Polyaniline (PANI) is considered as the most potential precursor because of its facile synthesis, environmental stability and high N/C ratio (0.167). PANI with various shapes has been produced[28–32] by controlling the synthesis conditions. Through high temperature heat treatment in an inert gas atmosphere, carbon nanostructures with special morphologies are easily prepared from the PANI nanostructures by maintaining the original shapes of PANIs.[14,15] A kind of nitrogen-doped hollow carbon spheres was synthesized by the use of sulfonated polystyrene spheres as a hard template.[22] The hard template method is common but complicated since the template must be removed and the structure of product may be destroyed. Therefore, it is necessary to develop a facile, cost-effective strategy for synthesizing heteroatom-doped hollow carbon spheres (HHCSs).

Herein, we report a method to prepare HHCSs *via* carbonization of hollow PANI spheres (HPSs). During the high temperature treatment, condensation and polymerization result in amorphous carbon with microporous and heteroatom-

[a]*National Engineering Center of Coal Water Slurry Gasification and Coal Chemical, Yankuang Group, Tengzhou, Shandong 277527, P. R. China*

[b]*State Key Laboratory of Chemical Resource Engineering, Beijing University of Chemical Technology, Beijing, 100029, P. R. China. E-mail: songhh@mail.buct.edu.cn; Fax: +86-010-64434916; Tel: +86-010-64434916*

doped structure. The obtained HHPSs show an excellent performance and rate capability as the electrode materials for supercapacitors. The excellent electrochemical performance is attributed to the heteroatom-doping and hollow carbon nanostructure of the HHCSs electrodes.

2. Experimental

2.1 Material

Aniline monomer, hydrogen peroxide (H_2O_2) (30 v/v% solution in water), ferric chloride hexahydrate ($FeCl_3 \cdot 6H_2O$), and sulfuric acid (H_2SO_4) were all AR grade (Tianjin Fuchen Chemical Reagents Factory, China). Aniline monomer was distilled before use under reduced pressure, and the other reagents were used as received without further purification. All the water used was ultrapure water (18.2 MΩ cm).

2.2 Synthesis of HHCSs

As shown in Fig. 1, a synthesis procedure was conducted to prepare HHCSs. PANI hollow spheres were synthesized by a one-pot polymerization. 0.5 mL of aniline monomer was dissolved in 150 mL of H_2SO_4 aqueous solution (0.15 M) with vigorous stirring at room temperature for several minutes to form a uniform solution. Then 0.5 mL of H_2O_2 and 10 mL of $FeCl_3$ (0.01 M) aqueous solution were mixed with the above solution in turn. After fully stirring, the mixture was transferred into a Teflon-lined stainless steel autoclave. The autoclave was sealed quickly and maintained at 150 °C for 6 h in an oven. Then, the autoclave was cooled to room temperature immediately by water cooling. The resulting product was collected by repeated centrifugation and washing in deionized water and ethanol. At last, the sample was dried in vacuum at 60 °C at least 6 h to obtain HPSs. The HPS was first put in the oven heating to 200 °C and kept at this temperature for 2 h in air. Then the HPS was heated to a predetermined value (600 °C, 700 °C and 800 °C) under a nitrogen atmosphere with a heating rate of 1 °C min^{-1}, and kept at this temperature for 2 h to obtain HHCSs-600, HHCSs-700 and HHCSs-800.

2.3 Characterization of materials

The obtained samples were investigated by scanning electron microscopy (SEM, ZEISS SUPRATM 55 field emission microscope), transmission electron microscopy (TEM, JEOL JEM-2100), and X-ray diffraction (XRD, Rigaku D/max-2500B2+/PCX) using Cu Kα radiation ($\lambda = 1.5406$ Å) over the range 5–90° (2θ) at room temperature. X-ray photoelectron spectra (XPS) were recorded on a Thermo Electron Corporation ESCALAB 250 XPS spectrometer using a monochromatized Al Kα radiation (1486.6 eV) with 30 eV pass energy in 0.5 eV step over an area of 650 μm × 650 μm to the sample. Nitrogen sorption isotherm was measured with ASAP2020 (Micromeritics, USA). Before sorption measurements, the samples were degassed at 300 °C for 6 h. Specific surface areas were estimated according to the BET model.

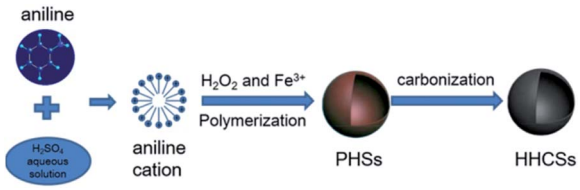

Fig. 1 A schematic illustration depicting the synthesis route for HHCSs.

2.4 Electrode assembly and measurement

The experiments were carried out in a standard three-electrode system, which contained a nickel foil electrode as a counter electrode, a Hg/HgO as a reference electrode, HHCSs loaded on foam nickel as a working electrode and KOH aqueous solution (6 M) as an electrolyte. Galvanostatic charge/discharge test was taken by CT2001A Battery Program Controlling Test System (China-Land Com. Ltd.) within a voltage range of −0.8 to 0 V, which was used to calculate the specific capacitance of HHCSs electrodes form the slope of discharge curves (dV/dt). The cyclic voltammetry and electrochemical impedance spectroscopy (EIS) were carried out on a ZAHNER ENNIUM (Germany) electrochemical working station. For the cyclic voltammetric measurements, the sweep rate ranged from 5 to 100 mV s^{-1} with a potential range of −0.8 to 0 V. For the EIS measurements, the frequency range was from 1 Hz to 10 kHz.

3. Results and discussion

The morphology of HPSs and HHCSs was detected by scanning electron microscopy (SEM) and transmission electron microscopy (TEM). It can be seen that the HPSs have a uniform spherical morphology (Fig. 2a). The TEM image (Fig. 2b) reveals the hollow sphere morphology of the HPSs. The diameter of the HPSs cavities and the thickness of the shells are about 600 nm and 100 nm, respectively. The formation mechanism of this kind of HPSs has been analyzed in previous reports.[33] Under this experimental condition, it is difficult to form a continuous supply of the building units due to the low concentration of micelles, and most of the micelles will assemble into original spheres through accretion. Afterward, these original spheres will react with newly produced O_2 bubbles driven by the oxidation–reduction reaction, or coalesce with each other and soluble micelles, resulting in formation of relatively uniform PHSs.

In order to get HHCSs, PHSs were heated in N_2 gas atmosphere at different temperatures from 600 to 800 °C. During the high temperature treatment, condensation and polymerization take place with the escape of hydrogen and nitrogen atoms, remaining the carbon skeleton. With increasing temperature, the non-carbon atoms lost more, and the carbon skeleton would gradually shrink. The shape of HHCSs-600 and HHCSs-700 generally maintains well after heat treatment (Fig. 2c and d). As shown in Fig. 2e, the shape of HHCSs-800 seriously shrinks. The spheres collapse and connect together. From Fig. 2f, the diameter of the HHCSs-700 cavities and the thickness of the shells are about 400 nm and 80 nm, respectively. A highly

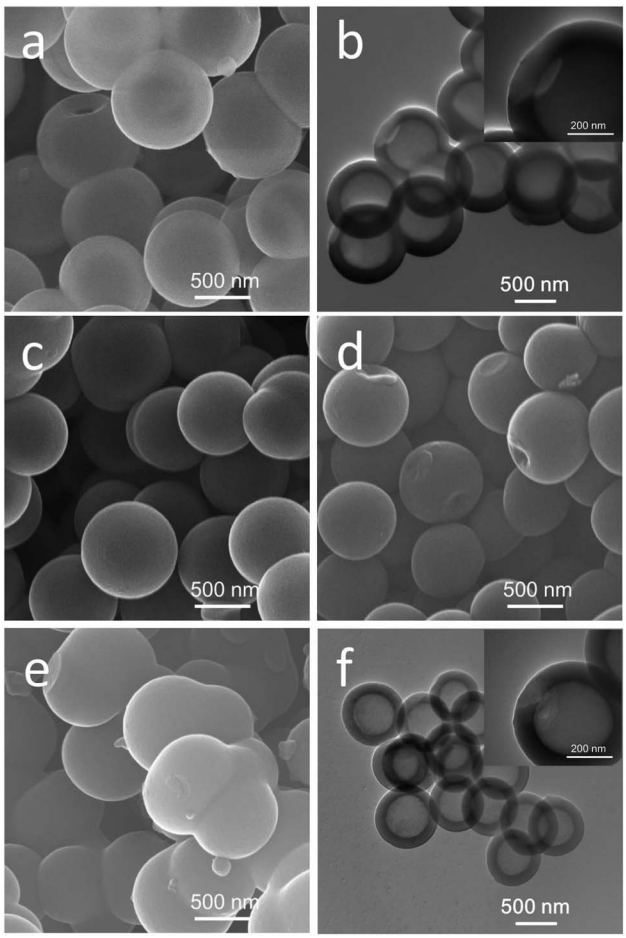

Fig. 2 SEM image of HPSs (a), TEM image of HPSs (b); SEM images of HHCSs-600 (c), HHCSs-700 (d) and HHCSs-800 (e); TEM image of HHCSs-700 (f).

developed microporous structure can form in HHCSs shell due to the pyrolysis and carbonization of the HPS. This unique porous hollow structure can provide a large specific surface area along with reduced diffusion lengths for both mass and charge transport.

Fig. 3 shows the XRD patterns of three samples. The XRD patterns of HHCSs exhibit one broad diffraction peak around 22°, which corresponds to the (002) facet of hexagonal graphitic carbon.[34–36] By increasing the carbonization temperature from 600 to 800 °C, the intensity of the peak slightly increased, suggesting the elevated degree of graphitization.

X-ray photoelectron spectroscopy (XPS) was employed to further analyze the nature and amount of functional groups of the HHCSs. The chemical state of nitrogen atoms in carbonized samples is assigned to five types according to previous reports:[37,38] 398.4 eV (pyridinic nitrogen N-6), 400 eV (pyrrolic nitrogen N-5), 401 eV (quaternary nitrogen N-Q) and 402.6 eV (pyridine-N-oxide or ammonia), and 405.5 eV (chemisorbed nitrogen oxides N-X). Some previous studies indicated that nitrogen located at the edges of graphene layers, for example, N-6 and N-5, could represent the pseudocapacitance effect.[16,39,40] N-6 enhances the capacitance owing to their positive charge, which allows fast electron transfer.[5,41]

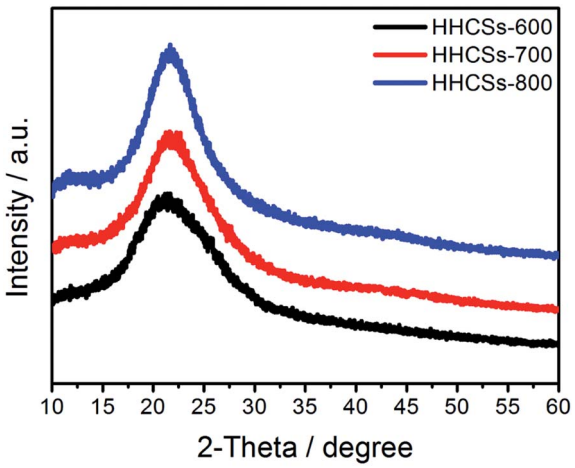

Fig. 3 XRD patterns of HHCSs.

Table 1 shows that the residual nitrogen content in the HHCSs is very high compared with those of other nitrogen-doped carbon materials.[33,34,42,43] It was found that the obtained materials have oxygen-containing functional groups as well as nitrogen functional groups, which are advantageous for capacitance as they can considerably contribute to an additional pseudo-capacitance.[44,45] Especially, oxygen functional groups can improve the wettability between electrode materials and electrolytes, depending on their hydrophilic nature.[46,47] The binding energies around 531.5 eV, 532.6 eV, and 533.7 eV represent C=O quinone type groups (O-1), C–OH phenol groups and/or C–O–C ether groups (O-2), and chemisorbed oxygen (COOH carboxylic groups) (O-3), respectively.[48,49] The following reactions of electroactive functional surface groups could be considered:[41,50]

$$>C\text{–}OH + OH^- \Leftrightarrow >C{=}O + H_2O + e^- \quad (1)$$

$$\text{–}COOH + OH^- \Leftrightarrow \text{–}COO^- + H_2O + e^- \quad (2)$$

In alkaline electrolytes, quinone groups are not electrochemically active, but carboxyl/phenol groups can react with OH^- to provide pseudocapacitance.[50–52] Hydroxyl groups and carboxyl groups have been found to be effective in improving carbon wettability and beneficial for electrolyte infiltration of

Table 1 The elemental composition and quantities (at%) of different energy levels atomic ratios for HHCSs obtained from XPS[a]

	Element content from XPS (at%)			% of total N 1s			% of total O 1s		
Sample	C	N	O	N-6	N-5	N-Q	O-1	O-2	O-3
HHCSs-600	81.9	7.4	10.7	37.5	16.4	46.1	35.9	46.8	17.3
HHCSs-700	83.4	7.3	9.3	28.2	16.6	55.1	29.7	36.3	34.0
HHCSs-800	88.3	4.8	6.9	8.5	45.3	46.2	18.9	48.2	32.8

[a] Pyridinic nitrogen (N-6), pyrrolic nitrogen (N-5), quaternary-N (N-Q). C=O quinone type groups (O-1), C–OH phenol groups and/or C–O–C ether groups (O-2), and chemisorbed oxygen (COOH carboxylic groups) (O-3).

the electrode. These two factors can improve the electrode capacitance and rate capability.[5,53]

XPS quantitative analysis reveals that the contents for nitrogen and oxygen species in HHCSs intensively depend on the pyrolysis temperature (see Fig. 4 and Table 1). When the pyrolysis temperature was increased from 600 to 800 °C, the heteroatom content decreased. As shown in Table 1, despite their different pyrolysis temperatures, all HHCSs possess a relatively higher amount of N-Q than N-5 and N-6 species. The content of N-6 decreases with the increase of pyrolysis temperature, especially between 700 °C and 800 °C, which is consistent with the previously reported studies.[54,55] Moreover, the content of O-1 decreases with the increase of pyrolysis temperature.

The specific surface area and porous properties are important for the electrode materials used in supercapacitors. The N_2 adsorption/desorption isotherms of HHCSs were shown in Fig. 5. The distinct hysteresis loops were found in the adsorption/desorption isotherms of HHCSs-600 and HHCSs-700, indicating the existence of mesoporous and microporous structures for HHCSs-600 and HHCSs-700. Table 2 shows that the HHCSs-700 possesses the highest surface areas and pore volume. Besides, it is found that HHCSs-800 possesses the lowest surface areas and pore volume. The decrease of surface areas in HHCSs-800 is due to the collapse of pores occurred at relatively high temperature. The specific surface area of the HHCSs-700 is 253 $m^2 g^{-1}$ and the total pore volume is 0.26 $cm^3 g^{-1}$. This can facilitate effective ion diffusion for the electrode.[34–36] The micropores of the HHCSs are favorable for enlarging the specific surface area, and mesopores offer larger channels for liquid electrolyte access and ion transport.

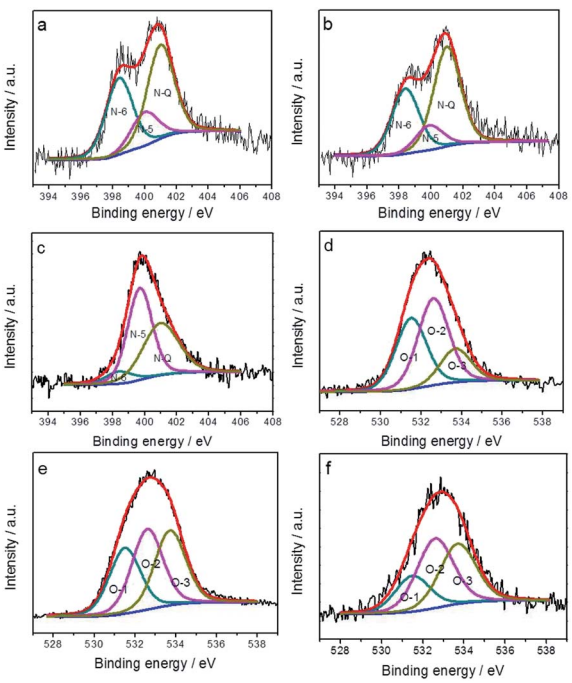

Fig. 4 N 1s spectra of (a) HHCSs-600, (b) HHCSs-700 and (c) HHCSs-800; O 1s spectra of (d) HHCSs-600, (e) HHCSs-700 and (f) HHCSs-800.

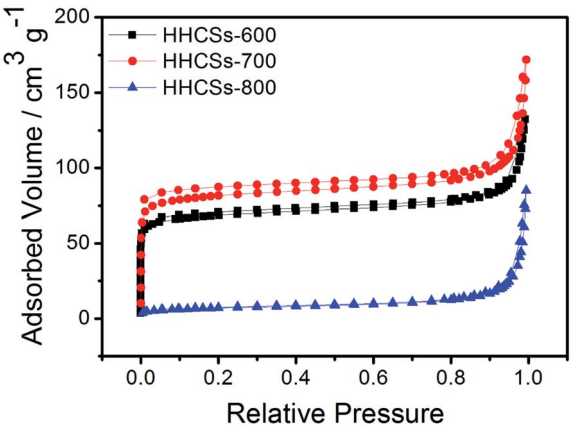

Fig. 5 N_2 adsorption/desorption isotherms of HHCSs.

Fig. 6a shows the CV curves of the HHCSs over a potential range from −0.8 to 0 V with a scanning rate of 50 mV s^{-1}. All the CV curves of HHCSs show rectangular-like shapes with broad redox peaks at low potentials, indicating that the electrodes possess both EDLC and faradaic capacitance.[56] The CV curves revealed that HHCSs-700 possessed the relatively highest specific capacitance because of its high heteroatoms content and high specific surface area. Fig. 6b shows the characteristic galvanostatic charge/discharge curves of HHCSs at the density of 0.5 A g^{-1}. The galvanostatic charge/discharge curves of HHCSs are not isosceles triangle due to the existence of pseudocapacitance. The specific capacitance of the HHCSs was evaluated according to the discharge time of galvanostatic charge/discharge. The discharge time of HHCSs-700 electrode is longer than that of HHCSs-600 and HHCSs-800 electrodes, indicating that HHCSs-700 possessed the relatively highest specific capacitance. The specific capacitances of HHCSs were calculated from galvanostatic discharge curves, and the comparison of the capacitance retention for HHCSs at a current density range from 0.5 to 10 A g^{-1} is presented in Fig. 6c. At a current density of 0.5 A g^{-1}, specific capacitances of 192, 241 and 67 F g^{-1} are obtained for HHCSs-600, HHCSs-700 and HHCSs-800 electrodes, respectively. The specific capacitance of HHCSs-700 is higher than that of the heteroatoms-doped carbon materials at the same current density.[15,33,34,42,43] To evaluate the cycle life of the HHCSs-700 for practical applications, the change of specific capacitance *versus* cycle number for the HHCSs-700 at a current density of 10 A g^{-1} is presented in Fig. 6d. Owing to the irreversible chemical reaction, the capacitance of HHCSs-700 decreases 8.5% after 10 cycles, but the capacitance decreases by only 3.6% after 10 000 cycles, indicating good cycling stability as an EDLC electrode material. The excellent performance of HHCSs-700 is attributed to the

Table 2 Porous properties of HHCSs

Samples	S_{BET} ($m^2 g^{-1}$)	V_{pore} ($cm^3 g^{-1}$)	$S_{t\text{-}potmicro}$ ($m^2 g^{-1}$)
HHCSs-600	199	0.19	153
HHCSs-700	253	0.26	191
HHCSs-800	26	0.13	5

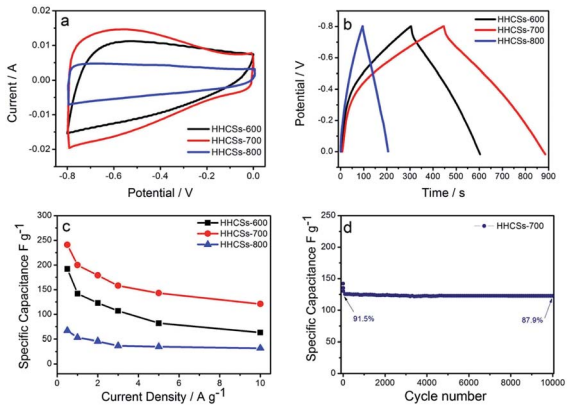

Fig. 6 (a) CV curves of HHCSs electrode at a scan rate of 50 mV s^{-1}. (b) Galvanostatic charge/discharge curves of the HHCSs electrode at the current density of 0.5 A g^{-1}. (c) Capacitance *versus* current density from 0.5 A g^{-1} to 10 A g^{-1} of HHCSs. (d) Cycling stability of the HHCSs-700 with a current density of 10 A g^{-1}.

combination of hollow spherical porous structure and the heteroatoms-doped carbon framework.[22,55]

EIS analysis is a powerful and informative technique to evaluate the properties of conductivity, structure and charge transport in the electrolyte interface.[57] Fig. 7 gives the curves of Nyquist plots of HHCSs electrodes in 6 M KOH aqueous solution. In the low-frequency region, HHCSs-700 electrode shows nearly a vertical line with higher slop suggesting that HHCSs-700 electrode has a Warburg resistance of charge saturation.[58] The slope of 45° portion of the curve in the medium frequency region indicates the characteristic of ion diffusion in the electrode structure. And the quasi-semicircle at high frequency suggests the charge-transfer resistance at the electrode–electrolyte interface. The charge transfer resistance of HHCSs-700 is extremely low from depressed semicircles, showing better capacitor behaviours.[59] The smaller impedances imply that the unique hollow nanostructure with well-developed porosity may facilitate fast ion and electrical charge transfer.

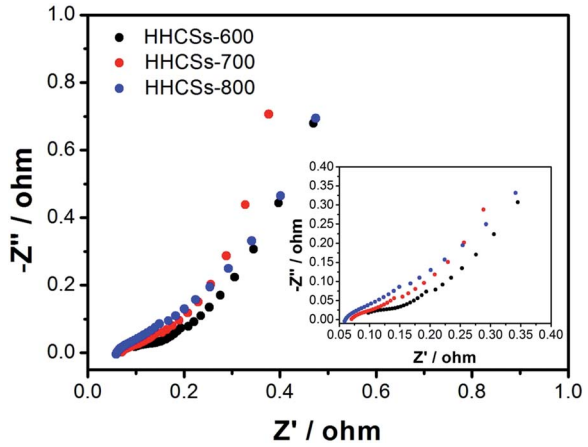

Fig. 7 Nyquist plots of HHCSs electrodes (the inset shows the expanded high-frequency region of the plots).

4. Conclusions

In summary, a kind of heteroatom-doped hollow carbon spheres has been prepared *via* direct carbonization of PHSs, which are synthesized by one-pot polymerization of PANI. It was found that the carbonized PHSs at 700 °C exhibits high specific capacitance and excellent rate capability. It is demonstrated that the appropriate heteroatom doping not only contributes to pseudo-capacitance but also improves the wettability of HHCSs in the electrolyte. This can enhance capacitance together with positive contribution from the hollow spherical porous structure. Therefore, the HHCSs-700 is a quite suitable and promising electrode material for supercapacitors.

Conflicts of interest

There are no conflicts to declare.

Acknowledgements

This work was supported by the Excellent Talents Supporting Program of Shandong province-administered enterprises of China.

Notes and references

1 Y. Zhai, Y. Dou, D. Zhao, P. F. Fulvio, R. T. Mayes and S. Dai, *Adv. Mater.*, 2011, **23**, 4828.
2 M. Winter and R. J. Brodd, *Chem. Rev.*, 2004, **104**, 4245.
3 S. Trasatti and P. Kurzweil, *Platinum Met. Rev.*, 1994, **38**, 46.
4 K. Kierzek, E. Frackowiak, G. Lota, G. Gryglewicz and J. Machnikowski, *Electrochim. Acta*, 2004, **49**, 515.
5 D. Hulicova-Jurcakova, M. Seredych, G. Q. Lu and T. J. Bandosz, *Adv. Funct. Mater.*, 2009, **19**, 438.
6 C. Portet, G. Yushin and Y. Gogotsi, *Carbon*, 2007, **45**, 2511.
7 Y. Liu, R. Deng, Z. Wang and H. Liu, *J. Mater. Chem.*, 2012, **22**, 13619.
8 W. Li, G. Reichenauer and J. Fricke, *Carbon*, 2002, **40**, 2955.
9 X. Yan, H. Song and X. Chen, *J. Mater. Chem.*, 2009, **19**, 4491.
10 M. Balathanigaimani, W.-G. Shim, M.-J. Lee, C. Kim, J.-W. Lee and H. Moon, *Electrochem. Commun.*, 2008, **10**, 868.
11 D. Bhattacharjya and J.-S. Yu, *J. Power Sources*, 2014, **262**, 224.
12 Y. S. Yun, S. Y. Cho, J. Shim, B. H. Kim, S. J. Chang, S. J. Baek, *et al.*, *Adv. Mater.*, 2013, **25**, 1993.
13 Y.-H. Lee, Y.-F. Lee, K.-H. Chang and C.-C. Hu, *Electrochem. Commun.*, 2011, **13**, 50.
14 D.-s Yuan, T.-x Zhou, S.-l Zhou, W.-j Zou, S.-s Mo and N.-n Xia, *Electrochem. Commun.*, 2011, **13**, 242.
15 M. Yang, B. Cheng, H. Song and X. Chen, *Electrochim. Acta*, 2010, **55**, 7021.
16 B. Xu, S. Hou, G. Cao, F. Wu and Y. Yang, *J. Mater. Chem.*, 2012, **22**, 19088.
17 M. Biswal, A. Banerjee, M. Deo and S. Ogale, *Energy Environ. Sci.*, 2013, **6**, 1249.
18 W. Huang, H. Zhang, Y. Huang, W. Wang and S. Wei, *Carbon*, 2011, **49**, 838.

19 V. Subramanian, C. Luo, A. Stephan, K. Nahm, S. Thomas and B. Wei, *J. Phys. Chem. C*, 2007, **111**, 7527.
20 X. He, P. Ling, M. Yu, X. Wang, X. Zhang and M. Zheng, *Electrochim. Acta*, 2013, **105**, 635.
21 Y. Ma, J. Zhao, L. Zhang, Y. Zhao, Q. Fan, L. Xa, *et al.*, *Carbon*, 2011, **49**, 5292.
22 J. Han, G. Xu, B. Ding, J. Pan, H. Dou and D. MacFarlane, Porous Nitrogen-Doped Hollow Carbon Spheres Derived from Polyaniline for High Performance Supercapacitors, *J. Mater. Chem. A*, 2014, **2**, 5352.
23 S. Peng, L. Li, H. Tan, R. Cai, W. Shi, C. Li, *et al.*, *Adv. Funct. Mater.*, 2014, **24**, 2155.
24 B. Fang, J. H. Kim, M.-S. Kim, A. Bonakdarpour, A. Lam, D. P. Wilkinson, *et al.*, *J. Mater. Chem.*, 2012, **22**, 19031.
25 B. You, J. Yang, Y. Sun and Q. Su, *Chem. Commun.*, 2011, **47**, 12364.
26 C. Dong, Z. Li, L. Zhang, *et al.*, *Diamond Relat. Mater.*, 2019, **92**, 32.
27 F. Ma, H. Zhao, L. Sun, Q. Li, L. Huo, T. Xia, S. Gao, G. Pang, Z. Shi and S. Feng, *J. Mater. Chem.*, 2012, **22**, 13464.
28 G.-R. Li, Z.-P. Feng, J.-H. Zhong, Z.-L. Wang and Y.-X. Tong, *Macromolecules*, 2010, **43**, 2178.
29 J. Han, P. Fang, J. Dai and R. Guo, *Langmuir*, 2012, **28**, 6468.
30 J. Huang and R. B. Kaner, *J. Am. Chem. Soc.*, 2004, **126**, 851.
31 Z. Zhou, J. Wang, Z. Wang and F. Zhang, *Mater. Lett.*, 2011, **65**, 2311.
32 E. N. Konyushenko, J. Stejskal, I. Šeděnková, M. Trchová, I. Sapurina, M. Cieslar, *et al.*, *Polym. Int.*, 2006, **55**, 31.
33 Y.-S. Zhang, W.-H. Xu, W.-T. Yao and S.-H. Yu, *J. Phys. Chem. C*, 2009, **113**, 8588.
34 G. Xu, B. Ding, P. Nie, L. Shen, J. Wang and X. Zhang, *Chem.–Eur. J.*, 2013, **19**, 12306.
35 G. Xu, B. Ding, P. Nie, L. Shen, H. Dou and X. Zhang, *ACS Appl. Mater. Interfaces*, 2013, **6**, 194.
36 G. Xu, B. Ding, L. Shen, P. Nie, J. Han and X. Zhang, *J. Mater. Chem. A*, 2013, **1**, 4490.
37 L. Qie, W. M. Chen, Z. H. Wang, Q. G. Shao, X. Li, L. X. Yuan, *et al.*, *Adv. Mater.*, 2012, **24**, 2047.
38 M. Sevilla, P. Valle-Vigón and A. B. Fuertes, *Adv. Funct. Mater.*, 2011, **21**, 2781.
39 X. Yang, D. Wu, X. Chen and R. Fu, *J. Phys. Chem. C*, 2010, **114**, 8581.
40 B. Xu, D. Zheng, M. Jia, G. Cao and Y. Yang, *Electrochim. Acta*, 2013, **98**, 176.
41 N. Mao, H. Wang, Y. Sui, *et al.*, *Nano Res.*, 2017, **10**, 1767.
42 L.-F. Chen, X.-D. Zhang, H.-W. Liang, M. Kong, Q.-F. Guan, P. Chen, *et al.*, *ACS Nano*, 2012, **6**, 7092.
43 L. Zhao, L. Z. Fan, M. Q. Zhou, H. Guan, S. Qiao, M. Antonietti, *et al.*, *Adv. Mater.*, 2010, **22**, 5202.
44 G. Pognon, T. Brousse and D. Bélanger, *Carbon*, 2011, **49**, 1340.
45 S. Roldán, C. Blanco, M. Granda, R. Menéndez and R. Santamaría, *Angew. Chem., Int. Ed.*, 2011, **50**, 1699.
46 L. Hao, X. Li and L. Zhi, *Adv. Mater.*, 2013, **25**, 3899.
47 Z. Lin, Y. Liu, Y. Yao, O. J. Hildreth, Z. Li, K. Moon, *et al.*, *J. Phys. Chem. C*, 2011, **115**, 7120.
48 M. Beidaghi and C. Wang, *Adv. Funct. Mater.*, 2012, **22**, 4501.
49 R. Arrigo, M. Hävecker, S. Wrabetz, R. Blume, M. Lerch, J. McGregor, *et al.*, *J. Am. Chem. Soc.*, 2010, **132**, 9616.
50 D. Hulicova-Jurcakova, M. Kodama, S. Shiraishi, H. Hatori, Z. H. Zhu and G. Q. Lu, *Adv. Funct. Mater.*, 2009, **19**, 1800.
51 B. Xu, S. Yue, Z. Sui, X. Zhang, S. Hou, G. Cao, *et al.*, *Energy Environ. Sci.*, 2011, **4**, 2826.
52 Y. Fang, B. Luo, Y. Jia, X. Li, B. Wang, Q. Song, *et al.*, *Adv. Mater.*, 2012, **24**, 6348.
53 Z. H. Huang, T. Y. Liu, Y. Song, *et al.*, *Nanoscale*, 2017, **9**, 13119.
54 R. Silva, D. Voiry, M. Chhowalla and T. Asefa, *J. Am. Chem. Soc.*, 2013, **135**, 7823.
55 C. Yuan, X. Liu, M. Jia, *et al.*, *J. Mater. Chem. A*, 2015, **3**, 3409.
56 X. Y. Chen, C. Chen, Z. J. Zhang, D. H. Xie, X. Deng and J. W. Liu, *J. Power Sources*, 2013, **230**, 50.
57 H. Liu, W. Zhang, H. Song, *et al.*, *Electrochim. Acta*, 2014, **146**, 511.
58 X. Ma, L. Gan, M. Liu, P. K. Tripathi, Y. Zhao, Z. Xu, D. Zhu and L. Chen, *J. Mater. Chem. A*, 2014, **2**, 8407.
59 W. Lu, M. Liu, L. Miao, *et al.*, *Electrochim. Acta*, 2016, **205**, 132.